Synergism between the Low-Level Jet and Organized Convection at Its Exit Region

CELESTE SAULO AND JUAN RUIZ

Centro de Investigaciones del Mar y la Atmósfera, CONICET, and Departamento de Ciencias de la Atmósfera y los Océanos, FCEyN, Universidad de Buenos Aires, Buenos Aires, Argentina

YANINA GARCÍA SKABAR

Centro de Investigaciones del Mar y la Atmósfera, CONICET, and Facultad de Agronomía, Universidad de Buenos Aires, Buenos Aires, Argentina

(Manuscript received 7 February 2006, in final form 30 May 2006)

ABSTRACT

Previous studies suggest that the enhanced meridional extent of some South American low-level jet events (known as Chaco jets) is a consequence of a positive feedback between the low-level wind and strong convection that is usually observed at their exit region. To assess how this interaction takes place, a Chaco low-level jet event observed between 18 and 19 December 2002 (i.e., during the South America Low-Level Jet Experiment) and the associated mesoscale convective system that evolved at its exit region have been selected to perform numerical experiments where diabatic heating effects associated with phase changes can be quantified. This case study has also been used to analyze the diurnal oscillations related to planetary boundary layer (PBL) mechanisms in order to describe whether the observed evolution of the low-level wind can be explained either by PBL-related forcing or by the interaction with convection. The sensitivity experiments confirm that there is a positive feedback at low levels between convection and the northerly wind flow that becomes accelerated and also aids in the identification of a strong coupling between organized convection and the upper-level circulation, resulting in an increase of the upper-level jet strength downstream of the simulated precipitation area. A conceptual model of how these systems (i.e., convection, low- and upper-level jets) mutually interact is proposed, which differs from coupling mechanisms documented for the Great Plains low-level jet.

1. Introduction

Recent studies related to the South America Low-Level Jet (SALLJ) have been focused on describing its mean features using gridded analyses (Marengo et al. 2004; Salio et al. 2002, and references therein), with an emphasis on the assessment of how this low-level wind flow affects the moisture balance of one of the richest agricultural basins in the world—the La Plata basin. Also, dynamical downscaling has been the choice to document the smaller-scale characteristics of this current, including its diurnal cycle (Saulo et al. 2000; Berbery and Collini 2000).

Given the lack of data over the region, fewer studies can be found providing observational evidence of the SALLJ and its variability (i.e., Fernandez and Necco 1982; Inzunza and Berri 1991; Douglas et al. 1998; Marengo et al. 2002). Some recent studies related to the processes that are responsible for this low-level jet (LLJ) include those by Paegle (1998) and Saulo et al. (2004) that concentrated mostly on local aspects of the jet and Campetella and Vera (2002) and Byerle and Paegle (2002) that focused on the larger-scale dynamics of the jet.

Geographical similarities between the Great Plains of North America (hereafter called simply the Great Plains) and the flat region east of the Andes and south of 20°S led to the idea that the main mechanisms driving the Great Plains LLJ should be also present in the SALLJ. While this hypothesis may be partially true, there are also important differences between the areas crossed by these jets (i.e., the topographical profile and the land surface characteristics) and between the predominant synoptic patterns characterizing the warm

Corresponding author address: Dr. Celeste Saulo, Centro de Investigaciones del Mar y Atmósfera, Facultad de Ciencias Exactas y Naturales, Ciudad Universitaria, Pabellón II, 2do piso, 1428 Buenos Aires, Argentina.
E-mail: saulo@cima.fcen.uba.ar

DOI: 10.1175/MWR3317.1

season weather over both continents that may account for significant changes in the behavior of the resulting low-level winds.

Paegle (1998) discusses possible reasons for different behavior between these two low-level jets. Among others, he mentions that the relative position of these jets with regard to the critical latitude (the latitude where the inertial oscillation period equals 24 h, i.e., 30°) is quite different, and a different diurnal phasing should be expected since most of the observations of SALLJ are at latitudes equatorward of 30°, while the Great Plains LLJ is mostly observed poleward of this latitude. He also mentions the effect of latent heat release over the mountains as an extra factor contributing to changing the differential heating profile between the slopes and the surrounding valleys. Using a very simple model that considers boundary layer oscillations superimposed with a dominant northerly geostrophic wind, Paegle (1998) partially explains some of the expected LLJ behavior, but stresses the discrepancies between the theoretical model and the few available observations.

Campetella and Vera (2002) and Byerle and Paegle (2002) further assess the role of the Andes in driving the mean low-level northerly flow, which is observed both in winter and summer (unlike what is observed in the Great Plains, where it occurs mainly in spring and summer). The former paper shows through idealized modeling experiments that the interaction of midlatitude baroclinic wave trains with the Andes topography is enough to reproduce some characteristics of the northerly low-level flow. On the other hand, Byerle and Paegle (2002) using monthly mean fields address the blocking effect of the Andes, which tends to produce an orographically bound cyclone that generates northerly low-level flow in both seasons, and also find that the amplitude of this vortex depends on the strength of the mean flow that crosses the Andes. Without an explicit focus on the LLJ, and using alternate idealized modeling experiments, Gandu and Geisler (1991) and Figueroa et al. (1995) show that the interaction of latent heat release due to Amazonian convection and the Andes topography explain many of the features related to low-level flow, particularly the ones that lead to convergence over the South Atlantic Convergence Zone (SACZ). It should be noted, however, that the circulation at low levels differs substantially between SACZ and non-SACZ regimes (Nogués-Paegle and Mo 1997). Since non-SACZ cases are closely related to stronger SALLJ events, these previous studies cannot fully explain the type of low-level circulation that is more relevant to this paper.

Saulo et al. (2004) used a case study approach to illustrate the different mechanisms that can be recognized during a particular LLJ event, characterized by an increased poleward penetration of the northerly wind. This kind of event, denoted by Nicolini and Saulo (2000) as a Chaco jet, has been related to an enhancement of precipitation over southeastern South America and consequently is of particular interest for the moisture budget of the La Plata basin. Saulo et al. (2004) concluded that during the life cycle of a Chaco jet event and along its path east of the Andes, local (planetary boundary layer) PBL-related effects (e.g., Blackadar 1957; Bonner and Paegle 1970; McNider and Pielke 1981) are only evident near the topography and only during the first day of the event. South of 25°S, the LLJ is synoptically driven and is mainly explained by a geostrophic response to the deepening of a thermal low over northwestern Argentina (Seluchi et al. 2003). At the exit region of the Chaco jet they find important ageostrophic components but not related to classical PBL–LLJ ones. They hypothesize that convection is responsible for these ageostrophic components, which lead to a larger meridional extent of the low-level wind flow.

To validate this hypothesis, this paper addresses the feedback mechanisms between the low-level jet and the organized convection at the exit region through a sensitivity experiment removing the effects of latent heat upon the simulated circulation. It should be stressed that the enhanced poleward extent of the northerly wind flow during particular SALLJ events is an aspect of the summer circulation that none of the idealized modeling studies cited before could reproduce.

While many studies can be found using this kind of methodology for different case studies over various parts of the world [Nicolini et al. (1993) and Chen et al. (1998) being closest to this study], no attempt to simulate this particular kind of feature and the synergism with the environmental circulation has been reported for South America. On the other hand, Chaco jet events account for more than 50% of the summer precipitation over southeastern South America (Salio et al. 2002), and this highlights the importance of understanding which are the preferred mechanisms of this relationship. This paper shows that through a relatively simple methodology, a conceptual model of how these systems mutually interact can be provided. The PBL-related forcing signature on the LLJ at particular sites has been identified, and similarities between this LLJ event and those reported in other parts of the world are also discussed.

The work is structured as follows: section 2 describes datasets and settings adopted to run the experiments with the Regional Atmospheric Modeling System

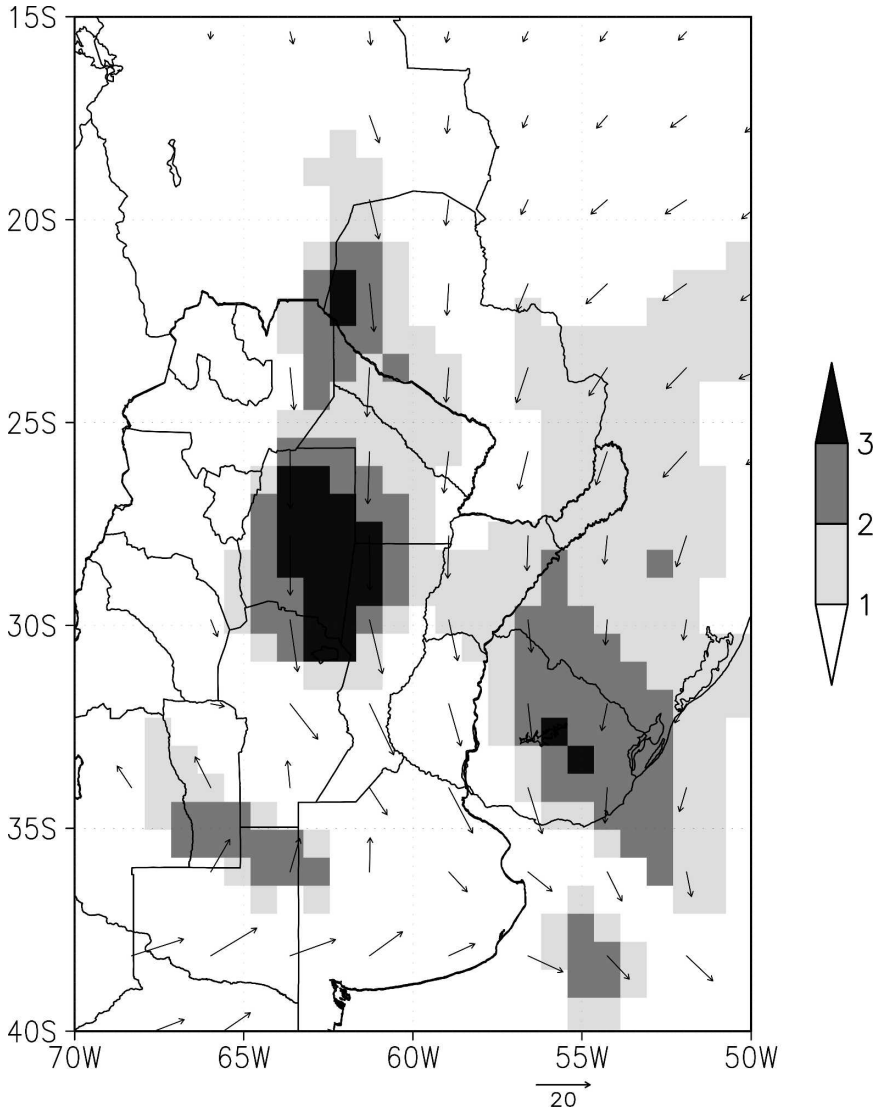

FIG. 1. Areas satisfying Bonner's criteria 1, 2, and 3 (shaded) and 850-hPa winds (vectors; m s^{-1}) after the 18-h simulation, valid at 0600 UTC 19 Dec 2002.

(RAMS); section 3 analyzes the synoptic situation, the PBL-related features of the LLJ, and the performance of the control run. The impact of removing latent heat effects is shown in section 4, while section 5 concentrates on the discussion of results.

2. Experimental design

As mentioned in the introduction, the event selected for the present study is denoted as a Chaco jet and has been identified following the criterion defined by Nicolini and Saulo (2000). The main characteristic of these particular South America low-level jet cases is their pronounced poleward penetration: the 12 m s^{-1} isotach at 850 hPa has to reach at least 25°S. Figure 1 corresponds to the time when this flow, observed on 19 December 2002, attained its maximum intensity (around 0600 UTC) and shows the areas where the Bonner (1968) criteria 1, 2, and 3 are met in the simulation. Bonner (1968) defines these criteria requiring that the wind at the maximum level must exceed 12, 16, and 20 m s^{-1}, respectively, and must decrease by at least 6, 8, and 10 m s^{-1}, respectively, to the next higher minimum or the 3-km level, whichever is lower. These criteria have been adapted to a gridded dataset at constant pressure levels, so that the same wind thresholds are required at any level below 850 hPa, and the same vertical wind shears are necessary between the level of

maximum wind and that of minimum wind (whenever this value is reached below 700 hPa).

The case under study has been selected among a set of events observed during the South America Low-Level Jet Experiment (SALLJEX; Vera et al. 2006) and occurred in conjunction with one of the largest mesoscale convective systems (MCSs) reported during this experiment (described in Ruiz et al. 2006), with a maximum areal extent of 500 000 km^2 at 0200 UTC 19 December 2002.

To capture the evolution of the low-level wind and the precipitation associated with the MCS, the numerical experiments started at 1200 UTC 18 December and ended at 1200 UTC 20 December 2002. RAMS version 4.3 has been used to simulate this event, using a low-resolution (80 km) domain covering South America with a higher-resolution (20 km) nested domain over the area of interest (Fig. 2). In all the experiments, the vertical resolution remained unchanged, with 30 sigma levels. The grid is a C-standard grid (Mesinger and Arakawa 1976) in polar stereographic projection. This nonhydrostatic version, which is similar to the one documented by Cotton et al. (2003), retains a better representation of atmospheric flow near steep topography (Tripoli and Cotton 1982) and also includes improvements to the shallow cumulus parameterization (Souza and Silva 2002) that complements the Grell cumulus parameterization (Grell 1993) adopted here. Turbulence parameterization follows the Smagorinsky (1963) treatment in the horizontal and Mellor and Yamada (1982) in the vertical, while long- and shortwave radiation are parameterized using the Chen and Cotton (1983) scheme.

Two experiments have been designed to assess the feedback between convection at the exit region of the LLJ and the circulation. The first one will be referred to as the control run (CR) and has been tuned so as to provide the best representation of the MCS–LLJ system. In this experiment, a two-way nesting between the high- and low-resolution grids has been performed. The CR initialization and boundary conditions have been derived from the Global Data Assimilation System [GDAS; the National Oceanic and Atmospheric Administration/National Centers for Environmental Prediction (NOAA/NCEP)] and encompass the whole domain (Fig. 2). The other experiment is denoted as the no-latent heat (NLH) run and has been performed as a one-way nesting (i.e., the boundary conditions for the high-resolution grid come from the low-resolution CR grid). In the NLH run, large-scale precipitation and convective parameterizations are disabled so that water vapor becomes a tracer inside the high-resolution domain, and consequently, latent heat release does not affect the thermodynamic equation. Moisture-related processes have been retained at the outer domain in order to restrict the area where the latent heat effect is removed; large amounts of precipitation occur over the northern portion of the domain (i.e., Amazonia) that can affect the circulation, although they are not related to the convection at the exit region of the LLJ. It should be noted that the resolution adopted for the experiments is not intended to resolve the circulation and the mesoscale characteristics of the MCS but is aimed at capturing the environmental conditions and the precipitation amounts related to the MCS.

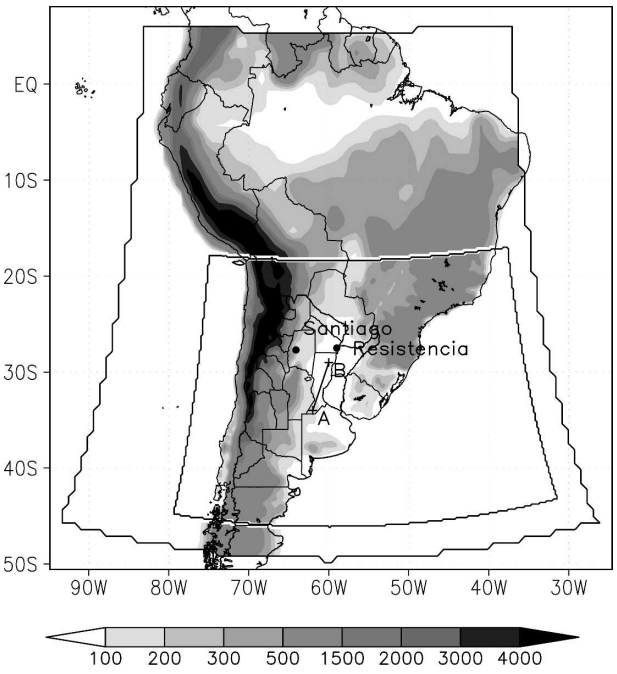

FIG. 2. Model domain (the inner domain corresponds to the nested area with higher resolution) and topography (m; shaded). Upper air stations and cross section mentioned in the text are indicated.

Precipitation and radiosonde datasets obtained from SALLJEX (Vera et al. 2006) have been employed to verify model performance, as well as GDAS gridded analyses. The selected event corresponds to a period within SALLJEX where only one radiosonde per day (at 0600 UTC) was launched at Resistencia (27°27′S, 58°59′W) and Santiago del Estero (27°48′S, 64°16′W; see Fig. 2 for station locations) while pilot balloon observations were available twice a day at Córdoba (31°25′S, 64°11′W), Chamical (30°22′S, 66°19′W), Joaquín V. González (25°04′S, 64°11′W), Pampa de los Guanacos (26°14′S, 61°52′W), Paraná (31°44′S, 60°32′W), Salta (24°47′S, 65°24′W), and Tostado (29°14′S, 61°47′W).

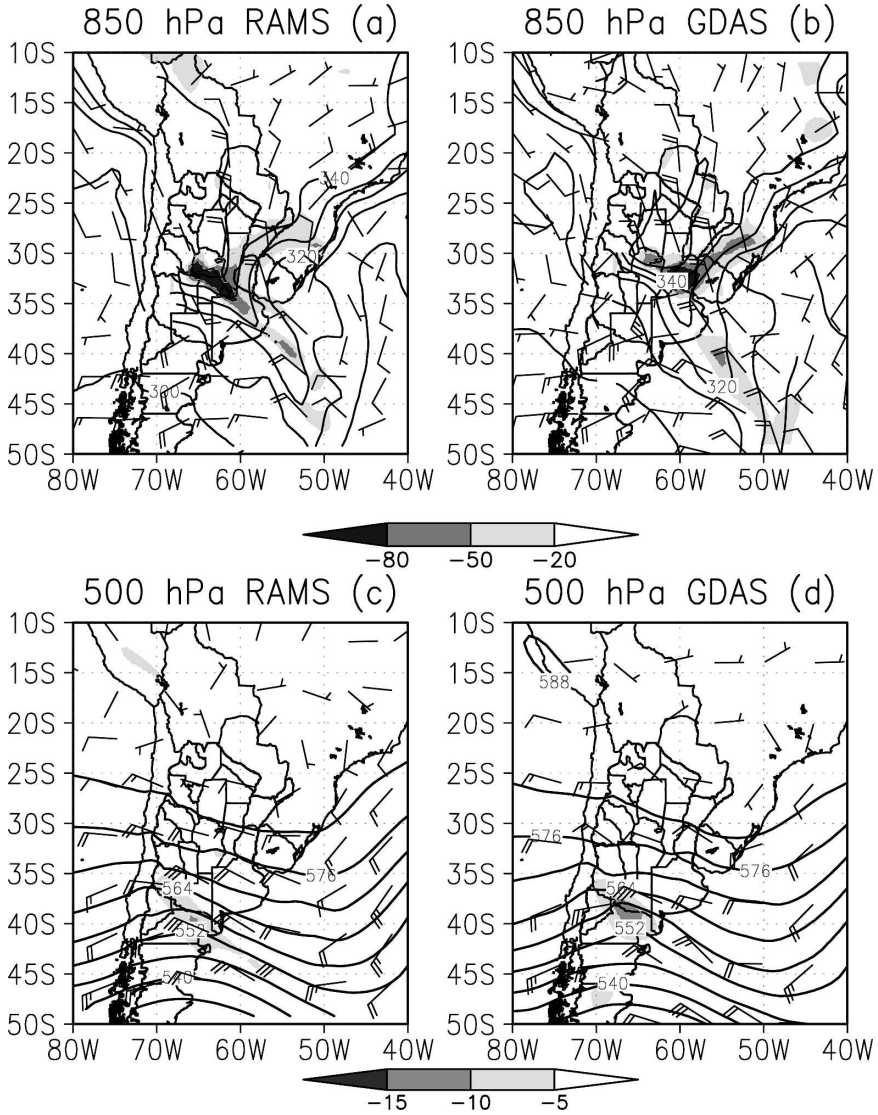

FIG. 3. (a), (b) 850-hPa equivalent potential temperature (K; contours), moisture divergence (10^{-8} s^{-1}; shaded), and wind vectors (m s^{-1}) and (c), (d) 500-hPa geopotential height (dam; contours), relative vorticity (10^{-5} s^{-1}; shaded), and wind barbs (m s^{-1}). All the fields correspond to 0600 UTC 19 Dec 2002 for CR (18-h simulation) and GDAS, respectively.

3. Characteristics of the 18 December 2002 Chaco jet event

a. Synoptic patterns and associated precipitation

The event under study exhibits an evolution similar to the one described by Saulo et al. 2004, except for a faster life cycle [northerly low-level wind satisfying Bonner (1968) criterion 1 is detected over central Argentina in the early morning of 18 December, while by 1800 UTC 19 December, the low-level flow reverses, being southerly over most of Argentina (not shown)]. The system first satisfies the Chaco jet condition (Nicolini and Saulo 2000) at 0000 UTC 19 December and the low-level northerly wind maximizes later, at 0600 UTC of the same day both in strength and areal coverage (Fig. 1).

Figure 3 provides a brief depiction of the main circulation features and how they are reproduced by RAMS CR at this time. At 850 hPa, northerly winds affect a region east of the Andes between 15° and 30°S, with maximum values above 20 m s^{-1} close to the Andes. Large amounts of moisture convergence associated with moist and warm advection are found in a band centered around 32°S ahead of a cold frontal zone oriented from WNW to ESE over central Argentina, which is noticeable by the equivalent potential tem-

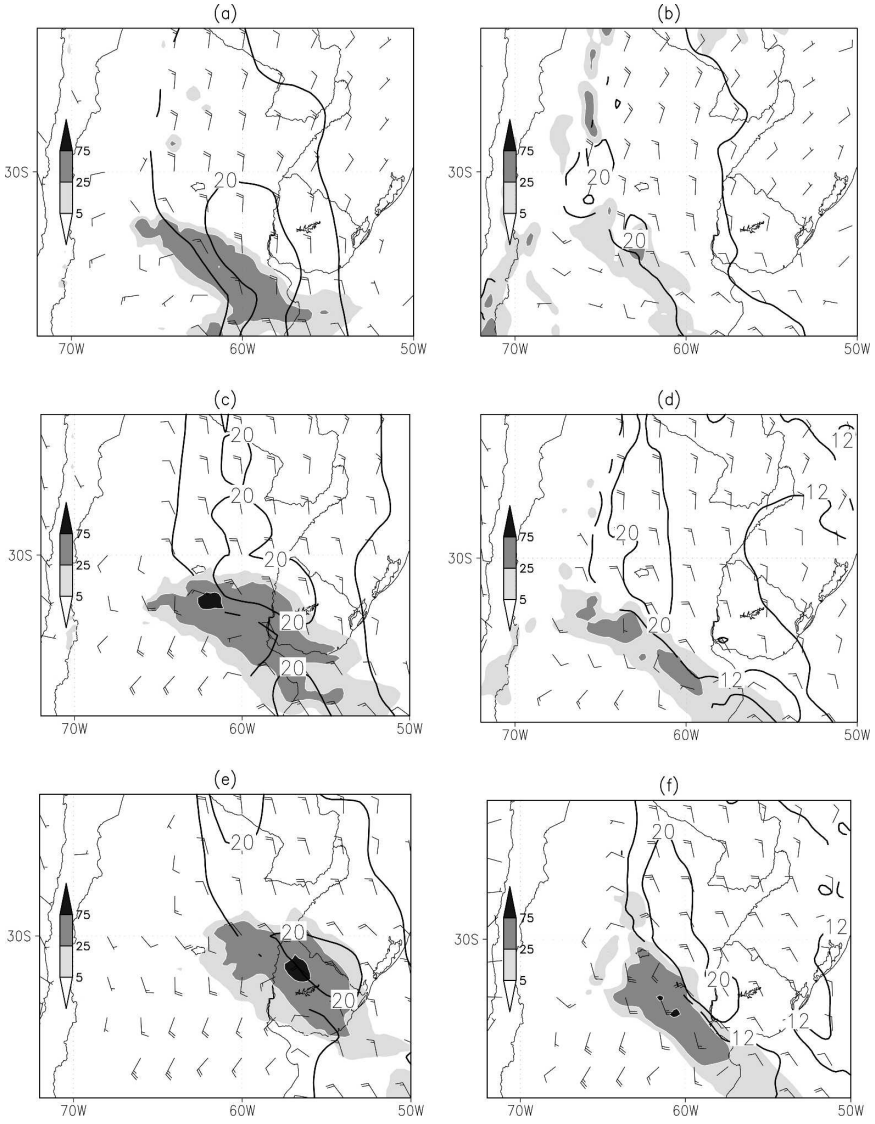

FIG. 4. Wind speed and wind vectors at 850 hPa, and 6-h total accumulated precipitation for (a), (c), (e) GDAS analysis and CMORPH precipitation estimates and (b), (d), (f) RAMS CR. Here, (a), (b) verify at 0000 UTC; (c), (d) at 0600 UTC; and (e), (f) at 12 UTC 19 Dec 2002.

perature contours. The maximum moisture convergence area is shifted toward the south and west in the CR with respect to GDAS, indicating that frontal velocity is lower in the 18-h simulation. The equivalent potential temperature gradient in the cross-front direction is slightly underestimated in the CR simulation.

The midlevel circulation (Figs. 3c,d) is characterized by a weak ridge centered at 50°W, downstream of the area where convection is occurring at this time (see Fig. 4), and a short-wave trough associated with the frontal zone is over southwestern Argentina. The position and intensity of these patterns are well captured by the model simulation, not only at this time but during the whole period of simulation (not shown).

Although MCS representation by the CR is not the focus of this paper, some related aspects will be shown with the aid of Fig. 4. The evolution of the 6-h accumulated precipitation associated with the MCS as derived from Climate Prediction Center (CPC) Morphing technique (CMORPH data; Joyce et al. 2004) and obtained with the CR, together with the 850-hPa winds, is included in this figure. The expected relationship between intense precipitation and the LLJ exit region location is suggested and this is well captured by the CR. The same holds for the representation of how the area covered by precipitation and the northerly wind intensity grow with time. Compared with CMORPH-derived precipitation, the CR underestimates rain intensity,

particularly at the developing stages of the system (Figs. 4a versus 4b). This can be partly explained by the fact that by 0000 UTC 19 December, the model is still within the spinup period. Also, the model rain area lags the one depicted by CMORPH data. Whether the lack of precision in the position of the low-level convergence zone (Figs. 3a,b) is a cause or an effect of the limitation of correctly representing the rain area is an issue that will be discussed later. However, some useful information about model drawback to capture convective initiation could be obtained through the inspection of surface temperature diurnal cycle (not shown)—CR failed to reproduce the higher temperatures observed over central Argentina by 2100 UTC 18 December, suggesting that there is an underestimation of low-level convective instability that can partially explain the model's inability to depict the earliest rains.

It should be noticed that CMORPH precipitation data are a derived product obtained from satellite imagery and as such should be used cautiously. Figure 5 compares the 24-h accumulated precipitation from three different sources: (i) simulated, (ii) observed, and (iii) derived from CMORPH. This figure essentially confirms what has been stated before—the first stages of the system are not well captured by the simulation (see the maximum observed over the Buenos Aires province around 61°W, 37°S), but the accumulated amounts are not far from observations; the model rain area lags the observed one, and CMORPH data tend to overestimate the area affected by precipitation (see, e.g., the maximum over Uruguay) and also the amounts. Unfortunately, the observational network exhibits significant gaps in coverage, while hourly data that could aid in determining some key features is nonexistent over the region. In addition, a model spinup period could not be avoided since this would require earlier initialization of model runs that produce a loss in model skill during the mature stage of the system. For these reasons, we opted to keep this experimental design under the assumption that the limitations in precipitation representation/location are not critical for our purposes.

The analysis of the 200-hPa level (Fig. 6) shows the expected strong divergent patterns associated with deep convection, which also seem to distort the upper-level jet strength and position. This feature, as well as the rest of the upper-level circulation patterns, is well captured by the model.

The environmental conditions associated with this Chaco jet event, as inferred from these figures, are similar to those documented in previous results (e.g., Salio et al. 2002; Saulo et al. 2004) and can be summarized as follows:

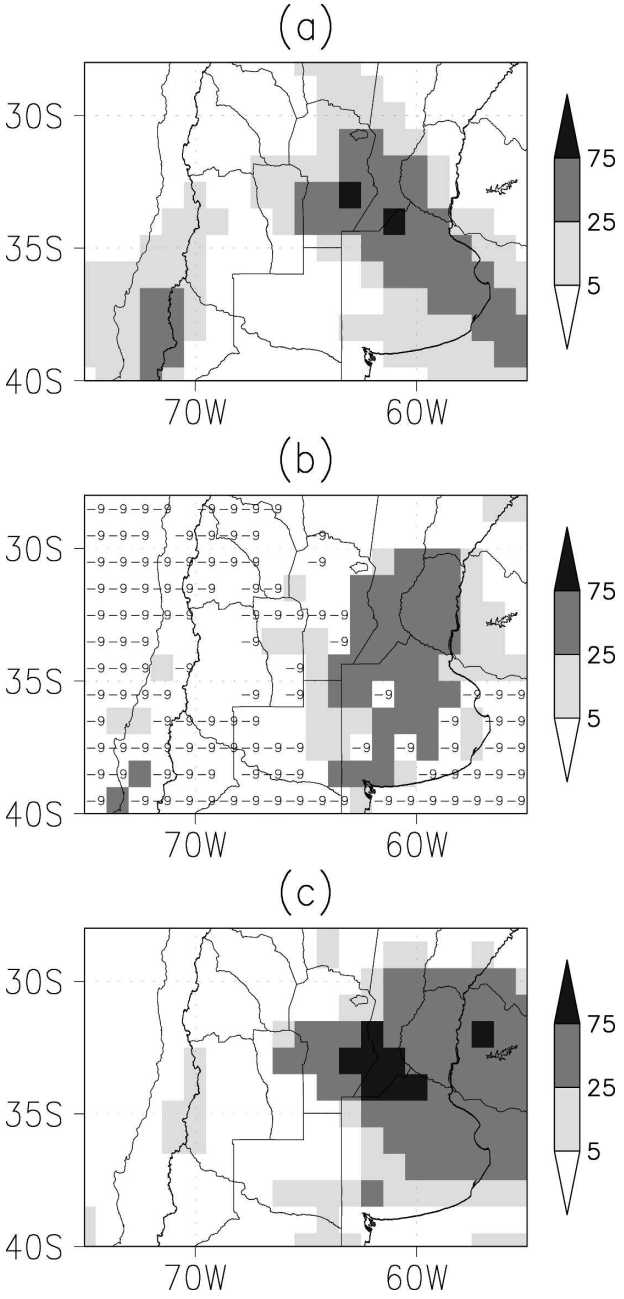

FIG. 5. Total accumulated precipitation between 1200 UTC 18 Dec and 1200 UTC 19 Dec 2002 in mm (filled boxes) (a) in the 24-h simulation, (b) observed in the SALLJEX rain gauge network, and (c) from CMORPH algorithm estimates. In (b), boxes without precipitation data are indicated with a −9. All datasets were interpolated to a 1° × 1° resolution.

- strong northerly winds at low levels, satisfying Bonner (1968) criteria, associated with warm and moist advection over a large area in southeastern South America (SESA),
- enhanced moisture convergence at low levels,
- propagation of a cold front from southern Argentina

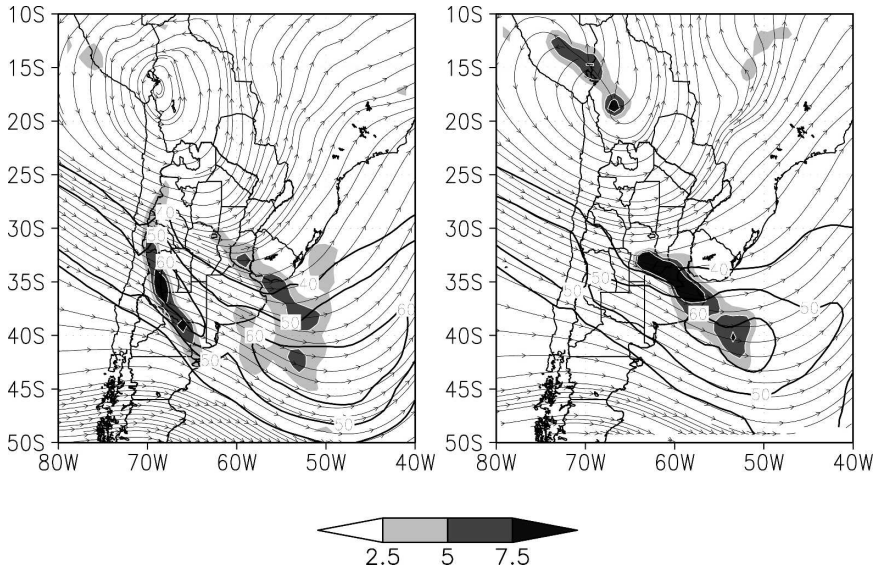

FIG. 6. Streamlines, isotachs (m s^{-1}), and divergence (10^{-5} s^{-1}; shaded) at 200 hPa for (a) the 18-h simulation and (b) GDAS, both valid at 0600 UTC 19 Dec 2002.

toward the northeast, which enhances the convergence at the exit region of the LLJ,
- baroclinic wave signature associated with the cold front propagation over the area: trough/ridge axis located over the central/eastern portion of the southern continent,
- strong precipitation at the exit region of the LLJ, and
- strong divergence at higher levels.

b. The low-level jet

The maximum extent of the area affected by LLJ conditions has been shown in Fig. 1. In this section, it is of interest to illustrate which of the well-documented PBL-related oscillations could be recognized in the present case. Figure 7 shows the expected nocturnal maximum in υ-wind speed at Santiago del Estero, as simulated with the CR (see Fig. 2 for station position), which reaches more than 20 m s^{-1} intensity between 0300 and 0900 UTC 19 December (corresponding to 0000 and 0600 LST) around 850 hPa. This figure also shows that the LLJ is immersed in a persistent northerly wind current that also undergoes synoptic variability (see, e.g., changes between 1200 UTC 18 and 19 December).

Blackadar's (1957) theory predicts an anticyclonic wind gyre as the day progresses, generated by the nocturnal reduction in stress, which leads to an acceleration in velocity as the wind field adjusts to a new balance with the existing pressure gradient. During this adjustment to the geostrophic wind, an inertial oscillation develops, in which the wind becomes supergeostrophic. The behavior of the υ-wind ageostrophic component in Fig. 7 (contours), which reverses from southerly to northerly as the day progresses into nighttime hours, is highly suggestive of the Blackadar (1957) mechanism. This feature could also be identified at other locations close to the mountains.

To better illustrate the anticyclonic wind gyre, the hodographs for the wind anomaly (defined as the actual wind minus the daily mean) at two different stations are presented in Fig. 8. In both cases, the wind exhibits the expected gyre, but the hodograph does not describe the classical ellipse documented by Bonner and Paegle

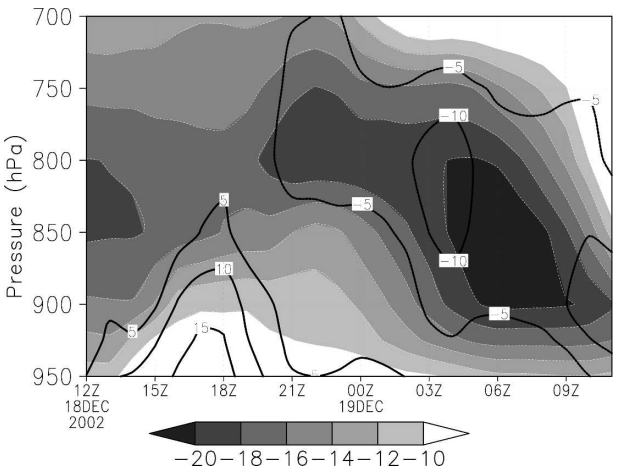

FIG. 7. Pressure vs time diagram displaying the simulated meridional wind (m s^{-1}; shaded) and meridional ageostrophic wind component (m s^{-1}; contours) at Santiago del Estero.

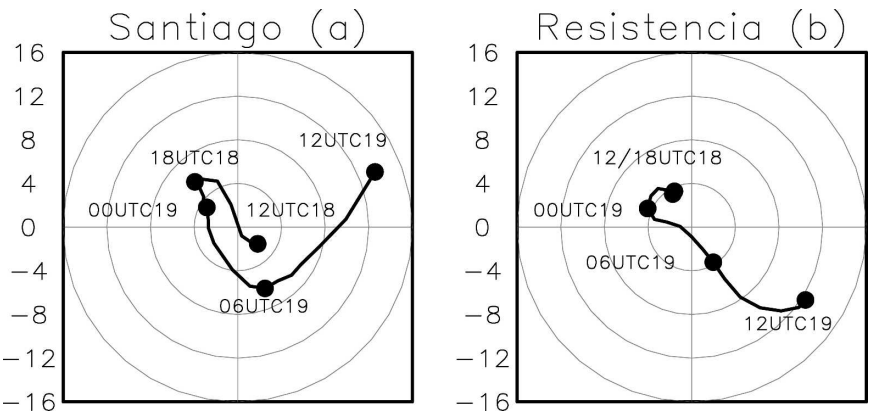

FIG. 8. The CR-simulated hodographs (with daily mean value removed) at 900 hPa from 1200 UTC 18 Dec to 1200 UTC 19 Dec 2002 for (a) Santiago del Estero and (b) Resistencia (see Fig. 2 for station location). Rings are every 3 m s^{-1}.

(1970) and also in later studies such as that by Zhong et al. (1996) for the Great Plains. In the latter, the authors mention that the behavior of the oscillation is "cleaner" at the LLJ core and more diffuse toward the east, that is, they obtain elliptical hodographs at the Neodesha and Lamont stations, while at DeQueen and Slater, the hodograph shows irregular oscillation patterns (see their Fig. 7). This explanation may hold for Resistencia (whose position is not within the LLJ core), but not for Santiago del Estero, which is located at the LLJ core. In this case, the hodograph is affected by the entrance of the cold front, as suggested by the southerly anomaly at 1200 UTC 19 December.

Unfortunately, SALLJEX special observations were taken only once a day through the dates of this episode, so the LLJ diurnal cycle cannot be validated using this additional dataset. Nevertheless, in order to provide an independent verification of the simulated wind profile, the SALLJEX radiosonde data at Santiago del Estero and Resistencia are plotted together with the GDAS analysis and the CR for the time when the LLJ was close to its maximum (Fig. 9). Two important aspects can be pointed out from this figure: the strength of the LLJ at both stations and the underestimation of its maximum by the GDAS analysis (particularly at Santiago del Estero), which is better represented by the CR. This figure reveals that the differences previously found in the low-level wind representation by GDAS and RAMS, particularly north of the convergence region (Fig. 4), may not necessarily be attributed to a model failure.

Following the hypothesis of Saulo et al. 2004, strong ageostrophic components unrelated to PBL oscillations should be found near the exit region of the LLJ, close to the area where precipitation is occurring. Consequently, this condition should be verified before progressing into the assessment of whether this circulation is actually driven by the convection.

Figure 10 shows the evolution of the wind and its ageostrophic component at various latitudes (longitudinally averaged around the core region of the LLJ). It is clear that soon after precipitation begins (by 2100 UTC 18 December), the ageostrophic northerly component increases and peaks by 0900 UTC 19 December, also following the maximum simulated precipitation. The rapid northward propagation of the cold front is also seen in this figure.

To quantitatively assess how the convection drives the observed circulation, the impact of removing the latent heat associated with precipitation is discussed in the following section.

4. The effect of latent heat release upon the simulated circulation

The impact of latent heat release, which is removed in the NLH run from the beginning of the experiment, becomes evident by 0000 UTC 19 December, after active areas of precipitation start to develop ahead of the surface convergent zone in the CR. Figure 11 illustrates low-level circulation and differences in the meridional wind at two times that are representative of this impact. For reference, the accumulated rain in the last hour (from CR) is included in all figures.

There are two main features that arise from this figure: northerly winds are stronger in the CR ahead of the precipitation area (i.e., to the north and northeast), and southerly winds are also stronger in the CR, thus promoting a faster frontal displacement (particularly close to the Andes) and supporting a stronger convergence at low levels as well as increasing frontogenesis. The area affected by the removal of latent heating is

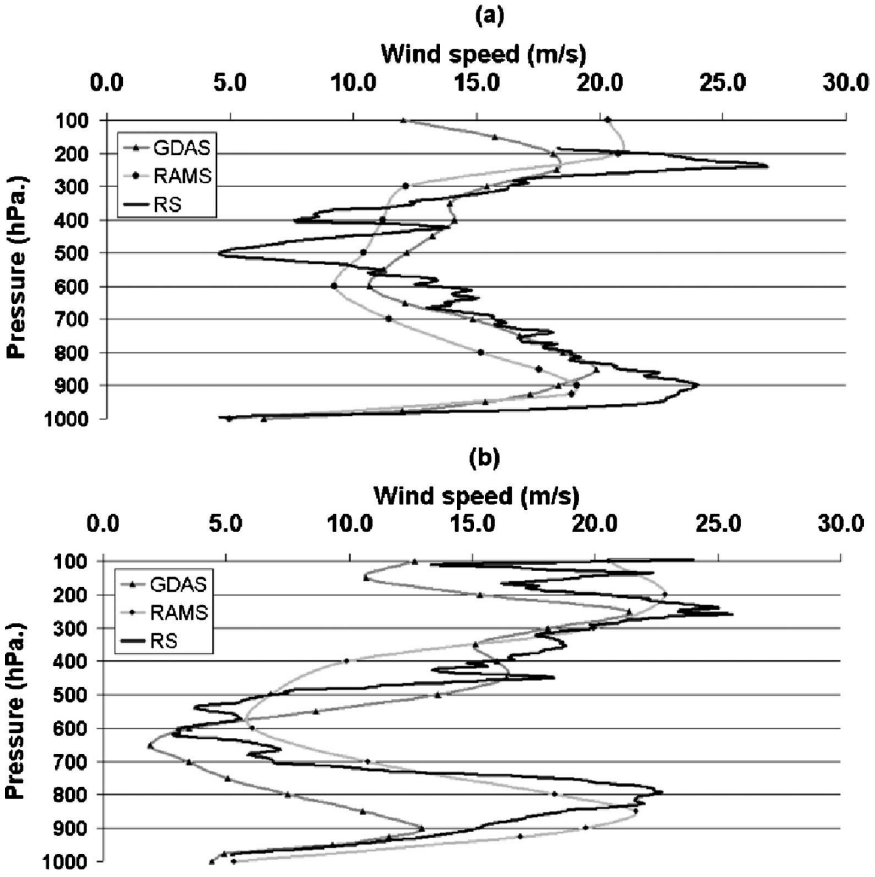

FIG. 9. Wind speed vertical profile at (a) Resistencia and (b) Santiago del Estero at 0600 UTC 19 Dec 2002 for GDAS (triangles), RAMS CR (circles), and radiosonde observations (solid line).

much larger than the area with precipitation and, as time progresses, differences associated with frontal position provoke the most evident changes at low levels. Note that contours correspond to v-wind differences, which are larger where the front has passed in the CR, while the NLH run still has northerly winds. Differences between these runs can also be used to give a plausible explanation for the lag between the simulated frontal position and the actual one, an aspect that has been pointed out in the previous section. The lack in the CR of correctly representing the precipitation, particularly at the beginning (between 1200 UTC 18 December and 0000 UTC 19 December), would lead to a decrease in both low-level convergence and frontogenesis.

The relative contribution of ageostrophic components to the low-level circulation will be discussed with the aid of Fig. 12. The larger differences in the ageostrophic northerly winds are collocated with the last-hour precipitation area and also over central and western Argentina. A very narrow band with southerly ageostrophic winds is also found just south of the rain area and is more evident at 1200 UTC. From the comparison of these figures, the effect of latent heat release upon the ageostrophic component of the northerly wind is verified while an effect on the southerly wind is also detected, both leading to an enhancement in low-level convergence. Ageostrophic winds in the NLH run (particularly evident over northeastern Argentina; Figs. 12b,d) behave as predicted by boundary layer dynamics (e.g., Paegle 1998) and rotate with the time of day, so that by 1200 UTC they become westerly while CR ageostrophic winds are still northerly. This is an indication of an adequate model representation of the diurnal wind oscillation (linked to PBL mechanisms) when convection as well as the synoptic variability associated with the faster frontal displacement found in the CR are prevented from interfering.

Besides the geostrophically unbalanced response already described, the wind also exhibits a balanced response to the latent heat release at low levels, which is seen in Fig. 13. Difference fields at 850 hPa denote the

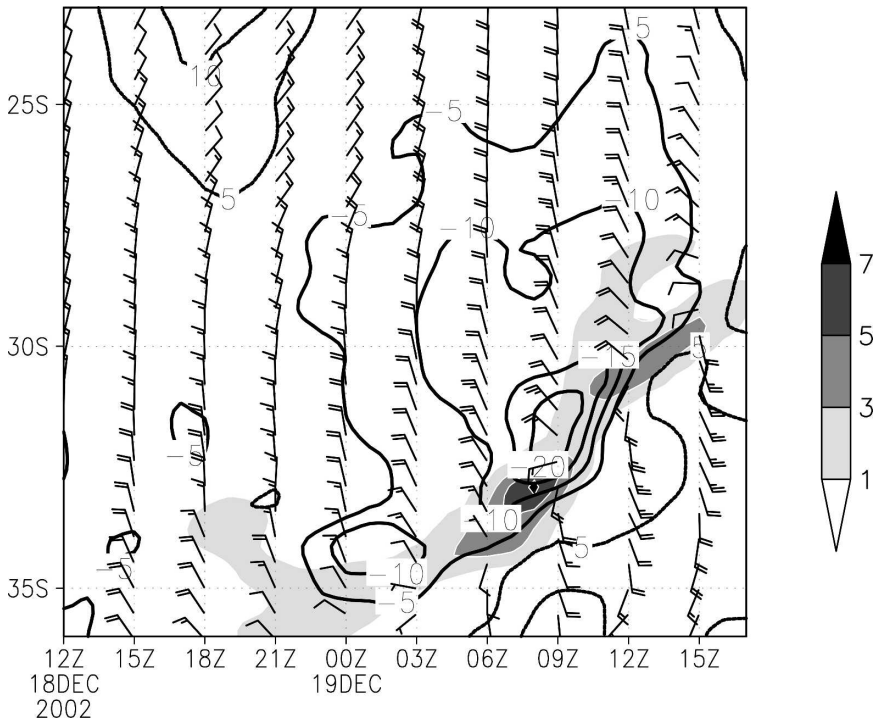

FIG. 10. Hovmöller diagram at 850 hPa of the vertically integrated condensate (mm; shaded), meridional ageostrophic wind (m s^{-1}; contours), and total wind (m s^{-1}; vectors) obtained with the CR and averaged between 60° and 63°W.

existence of a low pressure anomaly associated with a cyclonic circulation that also reinforces NW winds to the east and northeast of its center and SE winds to the west and southwest. This geostrophically balanced response of the motion field is noticed around the low pressure area, except over its center and close to the high topography, in accordance with the areas with stronger ageostrophic winds (Figs. 12a,c).

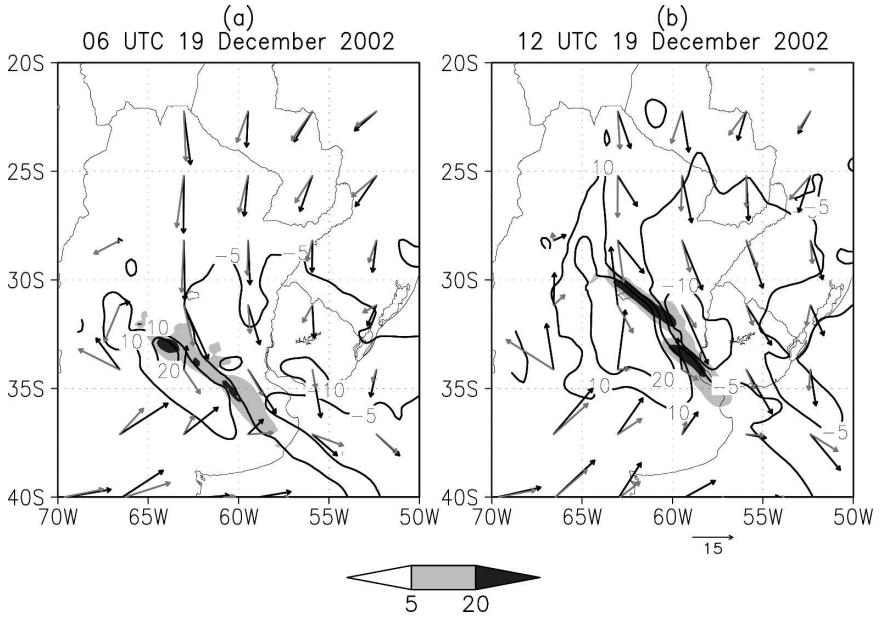

FIG. 11. The 850-hPa meridional wind difference (CR − NLH) (m s^{-1}; contours), total wind for the CR (m s^{-1}; black arrows) and the NLH run (m s^{-1}; gray arrows), and total rain in the last hour from CR (mm; shaded) at (a) 0600 UTC 19 Dec and (b) 1200 UTC 19 Dec 2002.

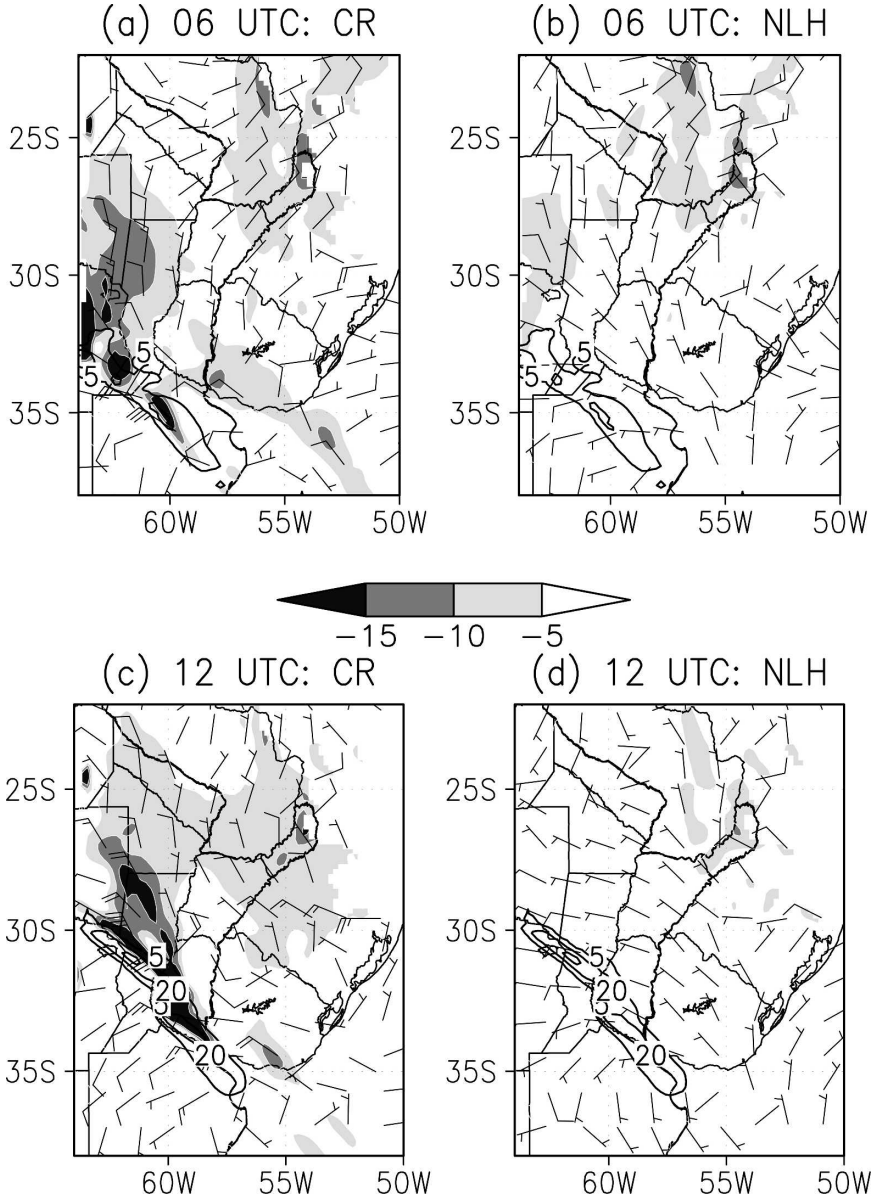

FIG. 12. The 850-hPa meridional ageostrophic wind (m s^{-1}; shaded), total ageostrophic wind (m s^{-1}; vectors), and last-hour accumulated rainfall (mm; contours) for the (a), (c) CR and (b), (d) NLH simulation. Here, (a), (b) correspond to the 18-h simulation verifying at 0600 UTC 19 Dec 2002 and (c), (d) to the 24-h simulation verifying at 1200 UTC 19 Dec 2002. Note that CR rainfall is included in NLH run plots just for reference.

Differences between runs are relatively weaker at 500 hPa and are mainly evidenced by the amplification of short-waves in the vorticity field (not shown). The similarity at this level between runs can be partially attributed to the fact that the simulated convective system in the CR does not produce a midlevel cyclone, which is a feature that should be expected in an MCS like this (Davis and Weisman 1994). As is further discussed in Ruiz et al. (2006), a possible explanation for the absence of a midlevel vortex is that the model fails to represent the stratiform region behind the convective line that, in turn, may be related to the lack of resolution of the experiments. On the other hand, provided that the latent heat release maximizes close to 500 hPa (see Fig. 14), the stronger impact should be expected above and below this level, as confirmed by the divergence patterns (area averaged following the MCS, as seen by the CR) and the associated geopoten-

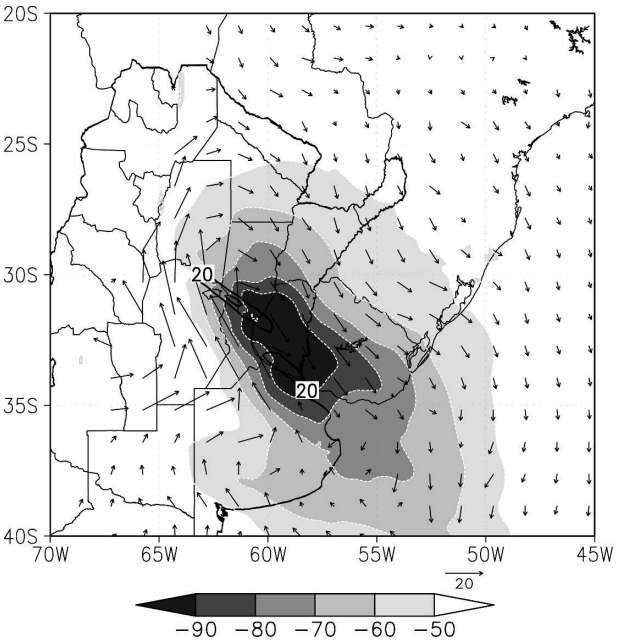

FIG. 13. The 850-hPa geopotential height difference (CR − NLH) (gpm; shaded), total wind difference (CR − NLH) (m s^{-1}; vectors), and last-hour accumulated rainfall (contours) verifying at 1200 UTC 19 Dec 2002.

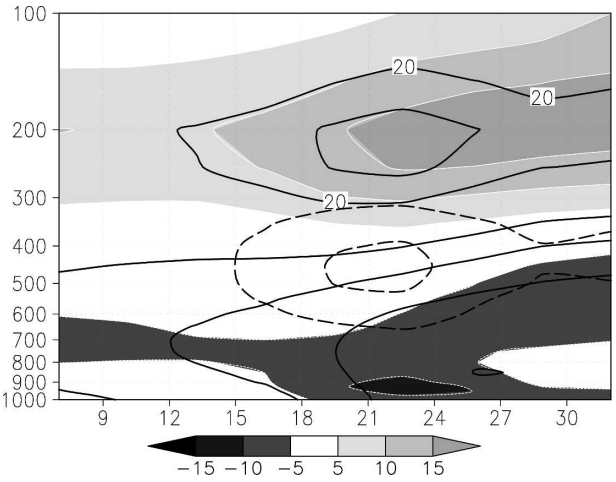

FIG. 14. Time vs pressure display of simulated divergence (CR) (10^{-6} s^{-1}; shaded), instantaneous heating rate associated with parameterized convection (CR) (dashed for 100 and 150 K day^{-1}), and geopotential height differences (CR − NLH) (mgp; contoured) averaged over a 2° × 2° box centered at the position of the maximun divergence at 200 hPa in the CR. Abscissas refer to simulation times, verifying between 1800 UTC 18 Dec and 1800 UTC 19 Dec 2002.

tial height differences between both runs. It is clear that the other striking impact is detected at 200 hPa as a response to the diabatic heating associated with convection, which is absent in the NLH run. The absence of divergence at upper levels clearly modifies the upper-level circulation, through a weakening of the upper-level jet streak intensity (cf. Figs. 6a and 15). Figure 16 corresponds to the time where this impact is larger and shows that at higher levels, the wind field anomaly is mostly unbalanced with respect to geostrophy; there is a subsynoptic-scale high pressure area, but wind differences are clearly divergent and promote an enhancement of the upper-level jet downstream (to the southeast) of the convective system. Though this response could be expected [see, e.g., Fritsch and Maddox's (1981) earlier work], the extent of the area affected by the convection-related circulation at upper levels is remarkable, with a half wavelength around 1600 km, meaning that its horizontal scale is similar to the Rossby radius of deformation (RRD), which is approximately 320 km. Following Pedlosky (2003), the RRD can be expressed as

$$\mathrm{RRD} = \frac{c_g}{f} \tag{1}$$

where c_g is the internal gravity wave speed (which, in turn, is a function of the Brunt–Väisälä frequency and the disturbance depth) and f is the Coriolis parameter.

The above analysis could be used to anticipate that this perturbation will alter the remote circulation and highlights the importance of reproducing these events for the improvement of the initial analysis and consequently of short-range weather prediction over this particular region.

Although the focus of the proposed experiment has been the impact of latent heating upon the circulation, it should be kept in mind that condensational warming is not the only diabatic effect that could have had a role upon the circulation. Another potential impact could be expected from the interaction between clouds and radiation. To disregard any other significant source of diabatic warming, heating rates associated with convection and radiation have been analyzed separately. Through this analysis (not shown), we corroborated that heating and cooling rates associated with radiation are around two orders of magnitude less than those associated with latent heat release throughout the simulation.

Figure 17 synthesizes the differences in the circulation between both runs (CR–NLH) along a transect perpendicular to the precipitation band (see Fig. 2 for transect position). Convective heating has been selected as a proxy for the position of the cloud system in the CR, coincident with the stronger simulated upward velocities. Associated with convergence at low levels and divergence at higher levels, two cells can be identified: one to the south with a direct circulation and

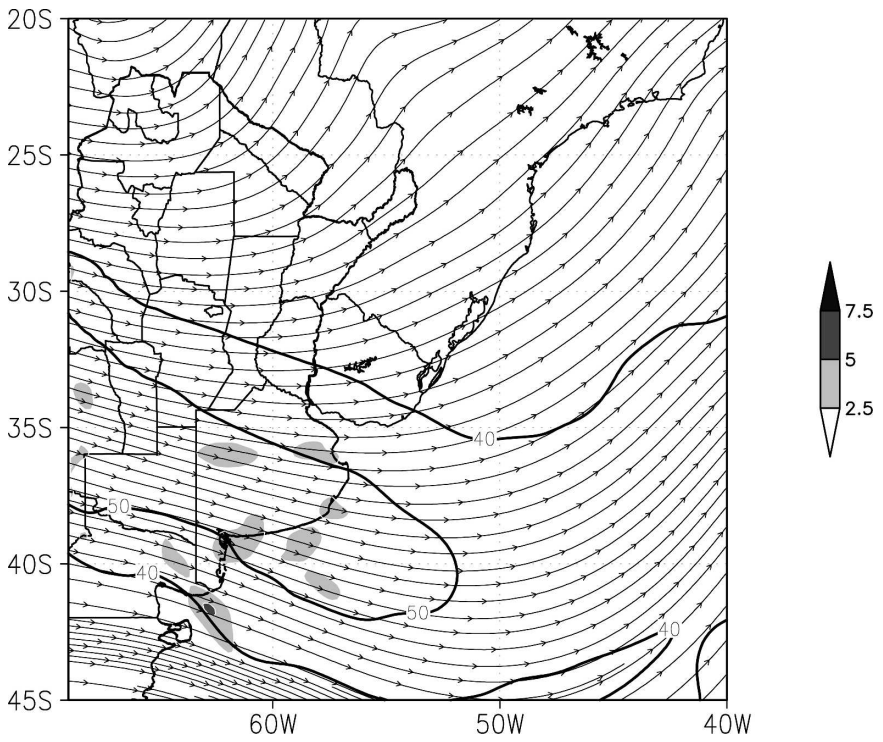

FIG. 15. Streamlines, isotachs (m s^{-1}), and divergence (10^{-5} s^{-1}; shaded) at 200 hPa for NLH verifying at 0600 UTC 19 Dec 2002.

another to the north (indirect), weaker than the previous one. It should be mentioned, however, that the transect orientation is such that the direct circulation (drawn using wind component along transect) seems to be stronger than the actual circulation strength.

5. Discussion of results

The case study presented here has been of aid for the identification of the synergism between the low-level jet and the organized convection at the exit region; warm and moist air convergence associated with the LLJ trigger and support convection, but latent heat release reinforces both northerly winds to the north and southerlies to the south so as to enhance convergence and guarantee a longer lifetime for the convective system. This kind of feedback has been reported by Nicolini et al. (1993) for the Great Plains LLJ. Yet, given the intense warming associated with large amounts of precipitation, this experiment has also revealed an important coupling with upper levels through an acceleration of the upper-level jet downstream of the heavy precipitation area and a weakening to the north.

The coupling between the LLJ and the upper-level jet has been addressed before, for example, in Uccellini and Johnson's (1979) paper. They present a basis for the dynamical processes responsible for coupling upper- and lower-tropospheric jet streaks through mutual mass–momentum adjustments and transverse circulations within the exit region of an upper-level jet streak. Their results are further supported by a climatology of 64 LLJs in the Great Plains where this coupling is confirmed (Chen and Kpaeyeh 1993). However, Chaco jets do not seem to respond to the referred coupling; their location is generally far from the exit region of the upper-level jet streak and more frequently observed near its entrance region (Salio et al. 2002).

Through a simple sensitivity experiment, it is possible to provide here an alternate explanation of the coupling between the LLJ and the upper-level jet in the presence of strong convection, as observed over southeastern South America. Figure 18 helps to illustrate the conceptual model proposed here.

The LLJ is the first feature to appear under the already defined environmental synoptic circulation and facilitates the organization of convection at its exit region. Then it becomes accelerated by the convection itself so that the fuel for convection is guaranteed through enhanced convergence at low levels for a longer time period. Convection, in turn, becomes deeper and better organized. As a result of the meso-

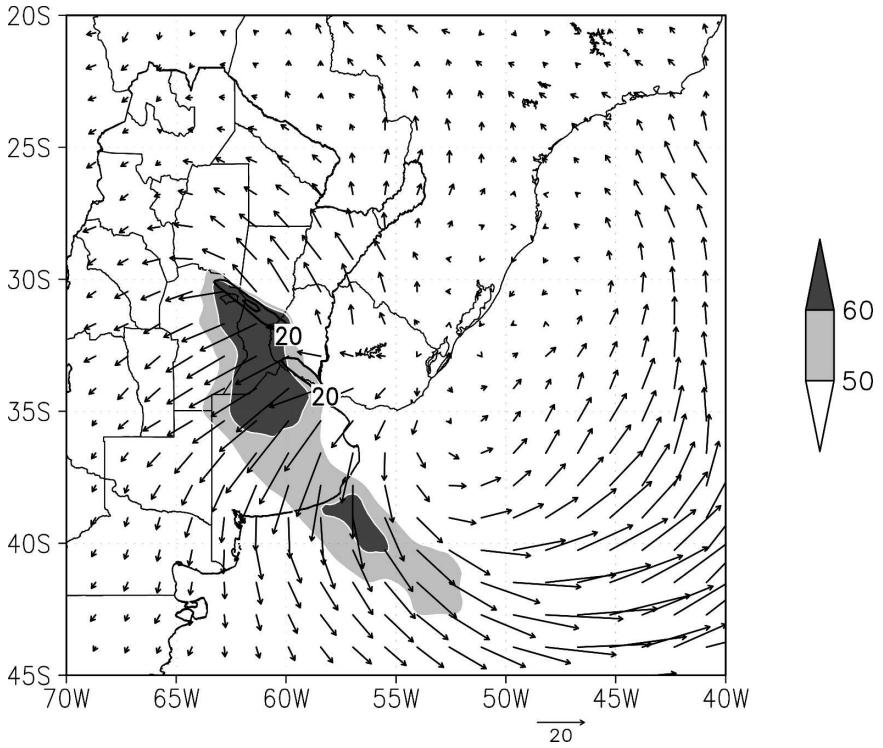

FIG. 16. Same as in Fig. 13, but for 200 hPa.

scale convective system that develops, a divergent flow dominates the wind pattern at higher levels and the upper-level jet is reinforced downstream through the generation of a direct cell to the south (stronger) and an indirect cell to the north (weaker) near the entrance region of the upper-level jet streak.

It is believed that this behavior dominates most of the Chaco jet events where strong convection occurs. As documented by Zipser et al. (2004), most of the MCSs observed during SALLJEX were associated with Chaco jet events, and a recent work by Salio et al. (2004) generalizes this result to other warm seasons. On the other hand, previous work by Nesbitt and Zipser (2003), Ferreira et al. (2003), and the seminal paper by Velasco and Fritsch (1987) also identify southeastern South America as a region with a high-frequency of occurrence of large MCSs. This would lead to the hypothesis that this region exhibits a particular (and mutually reinforced) interaction between extratropical dynamics and convection. Moreover, this particular case

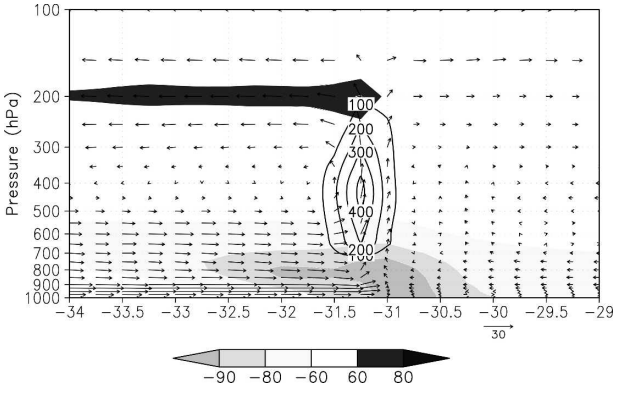

FIG. 17. Vertical cross section along A–B (Fig. 2) displaying geopotential height difference (CR − NLH) (gpm; shaded), tangential circulation differences (CR − NLH) (m s^{-1}; vectors), and instantaneous heating rate associated with parameterized convection (K day^{-1}) at 1200 UTC 19 Dec 2002.

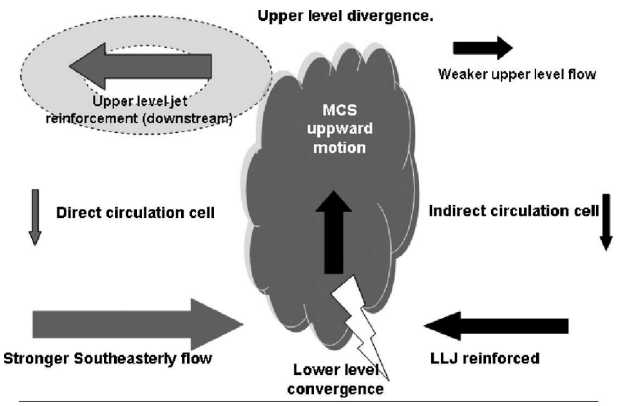

FIG. 18. Conceptual model describing the MCS and the induced circulation at the entrance region of the upper-level jet.

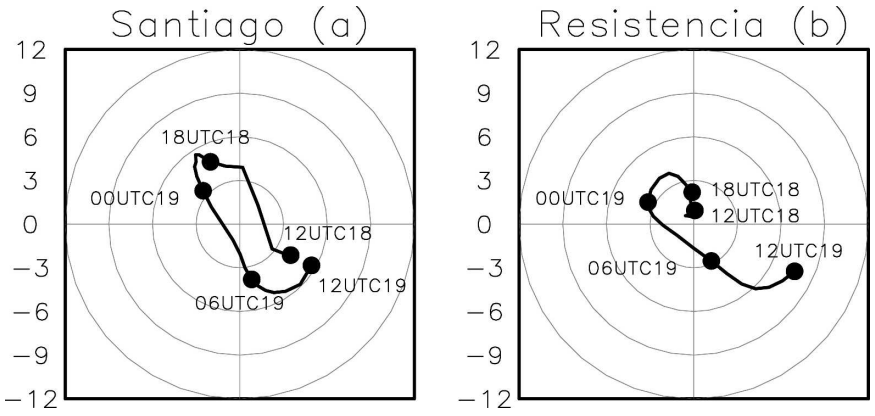

FIG. 19. Same as in Fig. 7, but for the NLH simulation.

study suggests that the mean upper-level field becomes modified even after the MCS has weakened and also drives attention toward the importance of correctly handling the assimilation of data that may depict the documented distortion of mass and wind fields and may be rejected by the analysis procedure.

This investigation also provides some evidence to explain why the PBL-related oscillations are only partially recognized during these kinds of events. Figure 19 is similar to Fig. 8 but derived from the NLH run. Now the hodographs are closer to the ellipse prescribed by the theory, particularly at Santiago del Estero, confirming the hypothesis that local PBL forcing is overridden by convection and larger-scale dynamics that occur concomitantly with Chaco jets. It should be mentioned that despite the lack of enough observations over the region and the fact that only one observation per day was available at the radiosonde stations for this case, SALLJEX data were useful to verify the model performance at individual points, which exhibited a good overall performance to represent the event.

Finally, it is of interest to mention that this kind of synergism between convection and circulation is more similar to that documented during a mei-yu front (Chen et al. 1998) than to that observed in the Great Plains LLJ, which may be mostly dominated by the Uccellini and Johnson (1979) kind of coupling. This similarity is surprising taking into consideration that the LLJ related to the mei-yu front exhibits a trajectory over warm waters (at least over much of its extent), thus explaining the huge amount of moisture available for the development of strong convection, and related circulation, although of smaller horizontal extent. The Chaco jet, in turn, has a continental path but through the Amazon basin, suggesting that this source of moisture is as efficient as tropical waters are to feed convection. On the other hand, the Great Plains LLJ is fed by the Gulf of Mexico moisture, but its trajectory over land is across very dry areas; thus, soil conditions seem to play a very different role on precipitation and its interaction with the LLJ (i.e., Zhong et al. 1996).The role of surface moisture upon the Chaco jet needs further assessment and will be the focus of future research.

Acknowledgments. We greatly appreciate Jan Paegle's comments on the manuscript. This study has been partially supported by the following projects: UBACyT X155 and X266, CONICET PIP 5417, ANPCyT PICT 25269, NOAA/OGP GC03-011, and ANPCyT PICT 2003 07-14420. SALLJEX has been supported by NOAA/OGP, NSF (ATM0106776), FAPESP Brazil (Grant 01/13816-1), ANPCYT PICT 07-06671, and UBACyT 055 Argentina.

REFERENCES

Berbery, E. H., and E. A. Collini, 2000: Springtime precipitation and water vapor flux over southeastern South America. *Mon. Wea. Rev.,* **128,** 1328–1346.

Blackadar, A. K., 1957: Boundary layer wind maxima and their significance for the growth of nocturnal inversions. *Bull. Amer. Meteor. Soc.,* **38,** 283–290.

Bonner, W. D., 1968: Climatology of the low level jet. *Mon. Wea. Rev.,* **96,** 833–850.

——, and J. Paegle, 1970: Diurnal variations in boundary layer winds over the south-central United States in summer. *Mon. Wea. Rev.,* **98,** 735–744.

Byerle, L., and J. Paegle, 2002: Description of the seasonal cycle of low-level flows flanking the Andes and their interannual variability. *Meteorologica,* **27,** 71–88.

Campetella, C. M., and C. S. Vera, 2002: The influence of the Andes Mountains on the South American low-level flow. *Geophys. Res. Lett.,* **29,** 1826, doi:10.1029/2002GL015451.

Chen, S., Y. Kuo, W. Wang, Z. Tao, and B. Cui, 1998: A modeling case study of heavy rainstorms along the Mei-Yu Front. *Mon. Wea. Rev.,* **126,** 2330–2351.

Chen, T. C., and W. R. Cotton, 1983: A one-dimensional simulation of the stratocumulus-capped mixed layer. *Bound.-Layer Meteor.,* **25,** 289–321.

——, and J. A. Kpaeyeh, 1993: The synoptic-scale environment associated with the low-level jet of the Great Plains. *Mon. Wea. Rev.,* **121,** 416–420.

Cotton, W. R., and Coauthors, 2003: RAMS 2001: Current status and future directions. *Meteor. Atmos. Phys.,* **82,** 5–29.

Davis, C. A., and M. L. Weisman, 1994: Balanced dynamics of mesoscale vortices produced in simulated convective systems. *J. Atmos. Sci.,* **51,** 2005–2030.

Douglas, M., M. Nicolini, and C. Saulo, 1998: Observational evidences of a low level jet east of the Andes during January–March 1998. *Meteorologica,* **23,** 63–72.

Fernandez, A., and G. Necco, 1982: Wind characteristics in the free atmosphere at Argentinean radiosounding stations (in Spanish). *Meteorologica,* **13,** 7–21.

Ferreira, R. N., T. M. Rickenbach, D. L. Herdies, and L. M. V. Carvalho, 2003: Variability of South American convective cloud systems and tropospheric circulation during January–March 1998 and 1999. *Mon. Wea. Rev.,* **131,** 961–973.

Figueroa, S. N., P. Satyamurty, and P. L. da Silva Dias, 1995: Simulations of the summer circulation over the South American region with an eta coordinate model. *J. Atmos. Sci.,* **52,** 1573–1584.

Fritsch, J. M., and R. A. Maddox, 1981: Convectively driven mesoscale weather systems aloft. Part I: Observations. *J. Appl. Meteor.,* **20,** 9–19.

Gandu, A. W., and J. E. Geisler, 1991: A primitive equations model study of the effect of topography on the summer circulation over tropical South America. *J. Atmos. Sci.,* **48,** 1822–1836.

Grell, G. A., 1993: Prognostic evaluation of assumptions used by cumulus parameterizations. *Mon. Wea. Rev.,* **121,** 764–787.

Inzunza, B. J., and G. J. Berri, 1991: Wind and vapor transport behavior in the lower troposphere over northern Argentina (in Spanish). *Meteorologica,* **17,** 17–25.

Joyce, R. J., J. E. Janowiak, P. A. Arkin, and P. Xie, 2004: CMORPH: A method that produces global precipitation estimates from passive microwave and infrared data at high spatial and temporal resolution. *J. Hydrometeor.,* **5,** 487–503.

Marengo, J. A., M. W. Douglas, and P. L. Silva Dias, 2002: The South American low-level jet east of the Andes during the 1999 LBA-TRMM and LBA-WET AMC campaign. *J. Geophys. Res.,* **107,** 8079, doi:10.1029/2001JD001188.

——, W. R. Soares, C. Saulo, and M. Nicolini, 2004: Climatology of the low-level jet east of the Andes as derived from the NCEP–NCAR reanalyses: Characteristics and temporal variability. *J. Climate,* **17,** 2261–2280.

McNider, R. T., and R. A. Pielke, 1981: Diurnal boundary-layer development over sloping terrain. *J. Atmos. Sci.,* **38,** 2198–2212.

Mellor, G. L., and T. Yamada, 1982: Development of a turbulence closure model for geophysical fluid problems. *Rev. Geophys. Space Phys.,* **20,** 851–875.

Mesinger, F., and A. Arakawa, 1976: Numerical methods used in atmospheric models. GARP Publ. 17, 64 pp.

Nesbitt, S. W., and E. J. Zipser, 2003: The diurnal cycle of rainfall and convective intensity according to three years of TRMM measurements. *J. Climate,* **16,** 1456–1475.

Nicolini, M., and A. C. Saulo, 2000: Eta characterization of the 1997–1998 warm season Chaco jet cases. Preprints, *Sixth Int. Conf. on Southern Hemisphere Meteorology and Oceanography,* Santiago de Chile, Chile, Amer. Meteor. Soc., 330–331.

——, K. M. Waldron, and J. Paegle, 1993: Diurnal oscillations of low-level jets, vertical motion, and precipitation: A model case study. *Mon. Wea. Rev.,* **121,** 2588–2610.

Nogués-Paegle, J., and K. C. Mo, 1997: Alternating wet and dry conditions over South America during summer. *Mon. Wea. Rev.,* **125,** 279–291.

Paegle, J., 1998: A comparative review of South American low level jets. *Meteorologica,* **23,** 73–81.

Pedlosky, J., 2003: *Waves in the Ocean and Atmosphere*. Springer-Verlag, 260 pp.

Ruiz, J., C. Saulo, Y. García Skabar, and P. Salio, 2006: The representation of a mesoscale convective system using RAMS model (in Spanish). *Meteorologica,* in press.

Salio, P., M. Nicolini, and A. C. Saulo, 2002: Chaco low-level jet events characterization during the austral summer season. *J. Geophys. Res.,* **107,** 4816, doi:10.1029/2001JD001315.

——, E. J. Zipser, M. Nicolini, and C. Liuct, 2004: Diurnal cycle of mesoscale convective systems over southeastern South America. *14th Int. Precipitation Cloud Conf.,* Bologna, Italy, 13–16.

Saulo, A. C., M. Nicolini, and S. C. Chou, 2000: Model characterization of the South American low-level flow during the 1997–1998 spring–summer season. *Climate Dyn.,* **16,** 867–881.

——, M. E. Seluchi, and M. Nicolini, 2004: A case study of a chaco low-level jet event. *Mon. Wea. Rev.,* **132,** 2669–2683.

Seluchi, M. E., A. C. Saulo, M. Nicolini, and P. Satyamurty, 2003: The northwestern Argentinean low: A study of two typical events. *Mon. Wea. Rev.,* **131,** 2361–2378.

Smagorinsky, J., 1963: General circulation experiments with the primitive equations. Part I: The basic experiment. *Mon. Wea. Rev.,* **91,** 99–164.

Souza, E. P., and E. M. Silva, 2002: Impact of the implementation of a shallow cumulus parameterization in a mesoscale model. Scheme description and sensitivity test (in Portuguese). *Rev. Bras. Meteor.,* **8,** 33–42.

Tripoli, G. J., and W. R. Cotton, 1982: The Colorado State University three-dimensional cloud/mesoscale model- Part I: General theoretical framework and sensitivity experiments. *J. Rech. Atmos.,* **16,** 185–220.

Uccellini, L., and D. Johnson, 1979: The coupling of upper and lower tropospheric jet streaks and implications for the development of severe convective storms. *Mon. Wea. Rev.,* **107,** 682–703.

Velasco, I., and J. M. Fritsch, 1987: Mesoscale convective complexes in the Americas. *J. Geophys. Res.,* **92,** 9591–9613.

Vera, C. S., and Coauthors, 2006: The South American Low-Level Jet Experiment. *Bull. Amer. Meteor. Soc.,* **87,** 63–77.

Zhong, S., J. D. Fast, and X. Bian, 1996: A case study of the Great Plains low-level jet using wind profiler network data and a high-resolution mesoscale model. *Mon. Wea. Rev.,* **124,** 785–806.

Zipser, E., P. Salio, and M. Nicolini, 2004: Mesoscale convective systems activity during SALLJEX and the relationship with SALLJ. *CLIVAR Exchanges,* No. 9, International CLIVAR Project Office, Southampton, United Kingdom, 14–16.